

Improved Measurement of the $b\bar{b}$ Production Cross Section in 920 GeV Fixed-Target Proton-Nucleus Collisions

I. Abt²³, M. Adams¹⁰, M. Agari¹³, H. Albrecht¹², A. Aleksandrov²⁹, V. Amaral⁸, A. Amorim⁸, S. J. Aplin¹², V. Aushev¹⁶, Y. Bagaturia^{12,36}, V. Balagura²², M. Bargiotti⁶, O. Barsukova¹¹, J. Bastos⁸, J. Batista⁸, C. Bauer¹³, Th. S. Bauer¹, A. Belkov^{11,†}, Ar. Belkov¹¹, I. Belotelov¹¹, A. Bertin⁶, B. Bobchenko²², M. Böcker²⁶, A. Bogatyrev²², G. Bohm²⁹, M. Bräuer¹³, M. Bruinsma^{28,1}, M. Bruschi⁶, P. Buchholz²⁶, T. Buran²⁴, J. Carvalho⁸, P. Conde^{2,12}, C. Cruse¹⁰, M. Dam⁹, K. M. Danielsen²⁴, M. Danilov²², S. De Castro⁶, H. Deppe¹⁴, X. Dong³, H. B. Dreis¹⁴, V. Egorytchev¹², K. Ehret¹⁰, F. Eisele¹⁴, D. Emeliyanov¹², S. Essenov²², L. Fabbri⁶, P. Faccioli⁶, M. Feuerstack-Raible¹⁴, J. Flammer¹², B. Fominykh²², M. Funcke¹⁰, Ll. Garrido², A. Gellrich²⁹, B. Giacobbe⁶, P. Giovannini⁶, J. Gläß²⁰, D. Goloubkov^{12,33}, Y. Golubkov^{12,34}, A. Golutvin²², I. Golutvin¹¹, I. Gorbounov^{12,26}, A. Gorišek¹⁷, O. Gouchtchine²², D. C. Goulart⁷, S. Gradl¹⁴, W. Gradl¹⁴, F. Grimaldi⁶, Yu. Gulinitsky^{22,35}, J. D. Hansen⁹, J. M. Hernández²⁹, W. Hofmann¹³, M. Hohlmann¹², T. Hott¹⁴, W. Hulsbergen¹, U. Husemann²⁶, O. Igonkina²², M. Ispiryan¹⁵, T. Jagla¹³, C. Jiang³, H. Kapitza¹², S. Karabekyan²⁵, N. Karpenko¹¹, S. Keller²⁶, J. Kessler¹⁴, F. Khasanov²², Yu. Kiryushin¹¹, I. Kisei²³, E. Klinkby⁹, K. T. Knöpfle¹³, H. Kolanoski⁵, S. Korpar^{21,17}, C. Krauss¹⁴, P. Kreuzer^{12,19}, P. Križan^{18,17}, D. Krücker⁵, S. Kupper¹⁷, T. Kvaratskhelia²², A. Lanyov¹¹, K. Lau¹⁵, B. Lewendel¹², T. Lohse⁵, B. Lomonosov^{12,32}, R. Männer²⁰, R. Mankel²⁹, S. Masciocchi¹², I. Massa⁶, I. Matchikhilian²², G. Medin⁵, M. Medinnis¹², M. Mevius¹², A. Michetti¹², Yu. Mikhailov^{22,35}, R. Mizuk²², R. Muresan⁹, M. zur Nedden⁵, M. Negodaev^{12,32}, M. Nörenberg¹², S. Nowak²⁹, M. T. Núñez Pardo de Vera¹², M. Ouchrif^{28,1}, F. Ould-Saada²⁴, C. Padilla¹², D. Peralta², R. Pernack²⁵, R. Pestotnik¹⁷, B. AA. Petersen⁹, M. Piccinini⁶, M. A. Pleier¹³, M. Poli^{6,31}, V. Popov²², D. Pose^{11,14}, S. Prystupa¹⁶, V. Pugatch¹⁶, Y. Pylypchenko²⁴, J. Pyrlik¹⁵, K. Reeves¹³, D. Reßing¹², H. Rick¹⁴, I. Riu¹², P. Robmann³⁰, I. Rostovtseva²², V. Rybníkov¹², F. Sánchez¹³, A. Sbrizzi¹, M. Schmelling¹³, B. Schmidt¹², A. Schreiner²⁹, H. Schröder²⁵, U. Schwanke²⁹, A. J. Schwartz⁷, A. S. Schwarz¹², B. Schwenninger¹⁰, B. Schwingenheuer¹³, F. Sciacca¹³, N. Semprini-Cesari⁶, S. Shuvalov^{22,5}, L. Silva⁸, L. Sözüer¹², S. Solunin¹¹, A. Somov¹², S. Somov^{12,33}, J. Spengler¹³, R. Spighi⁶, A. Spiridonov^{29,22}, A. Stanovnik^{18,17}, M. Staric¹⁷, C. Stegmann⁵, H. S. Subramania¹⁵, M. Symalla^{12,10}, I. Tikhomirov²², M. Titov²², I. Tsakov²⁷, U. Uwer¹⁴, C. van Eldik^{12,10}, Yu. Vassiliev¹⁶, M. Villa⁶, A. Vitale⁶, I. Vukotic^{5,29}, H. Wahlberg²⁸, A. H. Walenta²⁶, M. Walter²⁹, J. J. Wang⁴, D. Wegener¹⁰, U. Werthenbach²⁶, H. Wolters⁸, R. Wurth¹², A. Wurz²⁰, Yu. Zaitsev²², M. Zavertyaev^{12,13,32}, T. Zeuner^{12,26}, A. Zhelezov²², Z. Zheng³, R. Zimmermann²⁵, T. Živko¹⁷, A. Zoccoli⁶

¹NIKHEF, 1009 DB Amsterdam, The Netherlands ^a

²Department ECM, Faculty of Physics, University of Barcelona, E-08028 Barcelona, Spain ^b

³Institute for High Energy Physics, Beijing 100039, P.R. China

⁴Institute of Engineering Physics, Tsinghua University, Beijing 100084, P.R. China

⁵Institut für Physik, Humboldt-Universität zu Berlin, D-12489 Berlin, Germany ^{c,d}

⁶Dipartimento di Fisica dell' Università di Bologna and INFN Sezione di Bologna, I-40126 Bologna, Italy

⁷Department of Physics, University of Cincinnati, Cincinnati, Ohio 45221, USA ^e

⁸LIP Coimbra, P-3004-516 Coimbra, Portugal ^f

⁹Niels Bohr Institutet, DK 2100 Copenhagen, Denmark ^g

¹⁰Institut für Physik, Universität Dortmund, D-44221 Dortmund, Germany ^d

¹¹Joint Institute for Nuclear Research Dubna, 141980 Dubna, Moscow region, Russia

¹²DESY, D-22603 Hamburg, Germany

¹³Max-Planck-Institut für Kernphysik, D-69117 Heidelberg, Germany ^d

¹⁴Physikalisches Institut, Universität Heidelberg, D-69120 Heidelberg, Germany ^d

¹⁵Department of Physics, University of Houston, Houston, TX 77204, USA ^e

¹⁶Institute for Nuclear Research, Ukrainian Academy of Science, 03680 Kiev, Ukraine ^h

¹⁷J. Stefan Institute, 1001 Ljubljana, Slovenia ⁱ

¹⁸University of Ljubljana, 1001 Ljubljana, Slovenia

¹⁹University of California, Los Angeles, CA 90024, USA ^j

²⁰*Lehrstuhl für Informatik V, Universität Mannheim, D-68131 Mannheim, Germany*

²¹*University of Maribor, 2000 Maribor, Slovenia*

²²*Institute of Theoretical and Experimental Physics, 117259 Moscow, Russia*^k

²³*Max-Planck-Institut für Physik, Werner-Heisenberg-Institut, D-80805 München, Germany*^d

²⁴*Dept. of Physics, University of Oslo, N-0316 Oslo, Norway*^l

²⁵*Fachbereich Physik, Universität Rostock, D-18051 Rostock, Germany*^d

²⁶*Fachbereich Physik, Universität Siegen, D-57068 Siegen, Germany*^d

²⁷*Institute for Nuclear Research, INRNE-BAS, Sofia, Bulgaria*

²⁸*Universiteit Utrecht/NIKHEF, 3584 CB Utrecht, The Netherlands*^a

²⁹*DESY, D-15738 Zeuthen, Germany*

³⁰*Physik-Institut, Universität Zürich, CH-8057 Zürich, Switzerland*^m

³¹*visitor from Dipartimento di Energetica dell' Università di Firenze and INFN Sezione di Bologna, Italy*

³²*visitor from P.N. Lebedev Physical Institute, 117924 Moscow B-333, Russia*

³³*visitor from Moscow Physical Engineering Institute, 115409 Moscow, Russia*

³⁴*visitor from Moscow State University, 119899 Moscow, Russia*

³⁵*visitor from Institute for High Energy Physics, Protvino, Russia*

³⁶*visitor from High Energy Physics Institute, 380086 Tbilisi, Georgia*

[†]*deceased*

^a supported by the Foundation for Fundamental Research on Matter (FOM), 3502 GA Utrecht, The Netherlands

^b supported by the CICYT contract AEN99-0483

^c supported by the German Research Foundation, Graduate College GRK 271/3

^d supported by the Bundesministerium für Bildung und Forschung, FRG, under contract numbers 05-7BU35I, 05-7DO55P, 05-HB1HRA, 05-HB1KHA, 05-HB1PEA, 05-HB1PSA, 05-HB1VHA, 05-HB9HRA, 05-7HD15I, 05-7MP25I, 05-7SI75I

^e supported by the U.S. Department of Energy (DOE)

^f supported by the Portuguese Fundação para a Ciência e Tecnologia under the program POCTI

^g supported by the Danish Natural Science Research Council

^h supported by the National Academy of Science and the Ministry of Education and Science of Ukraine

ⁱ supported by the Ministry of Education, Science and Sport of the Republic of Slovenia under contracts number P1-135 and J1-6584-0106

^j supported by the U.S. National Science Foundation Grant PHY-9986703

^k supported by the Russian Ministry of Education and Science, grant SS-1722.2003.2, and the BMBF via the Max Planck Research Award

^l supported by the Norwegian Research Council

^m supported by the Swiss National Science Foundation

(The HERA-B Collaboration)

A new measurement of the $b\bar{b}$ production cross section in 920 GeV proton-nucleus collisions is presented by the HERA-B collaboration. The $b\bar{b}$ production is tagged via inclusive bottom quark decays into J/ψ mesons, by exploiting the longitudinal separation of $J/\psi \rightarrow l^+l^-$ decay vertices from the primary proton-nucleus interaction point. Both e^+e^- and $\mu^+\mu^-$ channels are reconstructed, for a total of 83 ± 12 inclusive $b \rightarrow J/\psi X$ events found. The combined analysis yields a $b\bar{b}$ to prompt J/ψ cross section ratio of $\frac{\Delta\sigma(b\bar{b})}{\Delta\sigma_{J/\psi}} = 0.032 \pm 0.005_{\text{stat}} \pm 0.004_{\text{sys}}$ measured in the x_F acceptance ($-0.35 < x_F < 0.15$), extrapolated to $\sigma(b\bar{b}) = 14.9 \pm 2.2_{\text{stat}} \pm 2.4_{\text{sys}}$ nb/nucleon in the total phase space.

PACS numbers:

13.85.Ni Inclusive production with identified hadrons

13.85.Qk Inclusive production with identified leptons, photons, or other non-hadronic particles

13.20.He Decays of bottom mesons

24.85.+p Quarks, gluons, and QCD in nuclei and nuclear processes

I. INTRODUCTION

Recent improvements in the theoretical description of heavy flavor ($c\bar{c}$, $b\bar{b}$) hadroproduction, inspired by the availability of increasing amount of data in various kinematic regimes, have provided new insight into the physics of hadron-hadron collisions [1, 2]. Investigations in this field are further stimulated by the current and the next generation of heavy ion colliders (RHIC, LHC) where signatures of Quark Gluon Plasma (QGP) can be identified only after hadron-hadron collisions in a non-QGP regime are understood with sufficient accuracy.

In the field of fixed target bottom production, several experiments have been performed over the past years at Fermilab, CERN and DESY with both pion and proton beams (see [3, 4, 5] for recent reviews). Several theoretical calculations have become available [6, 7], although the accuracy of the predictions is usually quite poor. The large experimental and theoretical uncertainties provide a strong motivation for a more precise and accurate measurement of near-threshold $b\bar{b}$ production, where the sensitivity to theoretical models is large and the kinematic region is complementary to that of $c\bar{c}$ or $b\bar{b}$ production at very high energies at collider experiments. In fact, in the near-threshold region, perturbative QCD can be applied and full next-to-leading-order calculations are available, although higher order terms are important and not yet fully evaluated. In this regime, measurements have been published by only three experiments: E789 [8], E771 [9] and HERA-B [10].

The HERA-B experiment can measure the $b\bar{b}$ cross section via the inclusive $b \rightarrow J/\psi X$ decay mode. Interactions are produced by 920 GeV protons in the halo of the HERA beam impinging on target wires of different materials at $\sqrt{s} = 41.6$ GeV proton-nucleon center-of-mass energy. The $b\bar{b}$ production cross section ($\sigma_{b\bar{b}}^A$) on a nucleus of atomic number A is obtained via the inclusive reaction

$$pA \rightarrow b\bar{b} X \text{ with } b\bar{b} \rightarrow J/\psi Y \rightarrow (e^+e^-/\mu^+\mu^-)Y.$$

The b hadrons decaying into J/ψ (“ $b \rightarrow J/\psi$ ” in the following) are distinguished from the large background of J/ψ mesons produced directly on the target (“prompt J/ψ ” in the following) by exploiting the b lifetime in a detached vertex analysis. HERA-B is capable of detecting both dilepton decay channels of the J/ψ , providing an increase of the statistical significance of the measurement and internal consistency checks.

A first measurement based on limited statistics was published in [10]. This work presents an improved measurement based on larger statistics collected during the 2002-2003 data taking. The larger sample of $b\bar{b}$ events allows us to perform further cross checks, such as a lifetime measurement, a search for specific decay channels of B mesons with a J/ψ in the final state and a search for inclusive decays of the form $b \rightarrow J/\psi + h^\pm + X$.

The present paper is structured as follows. In Sect. II the basic concepts of the $\sigma(b\bar{b})$ measurement are discussed. An overview of the detector, the trigger performance and the data samples is given in Sect. III, followed by a description of the Monte Carlo simulation (Sect. IV). The methods used for the J/ψ reconstruction and selection are presented in Sect. V and discussed separately for the muon ($J/\psi \rightarrow \mu^+\mu^-$) and the electron ($J/\psi \rightarrow e^+e^-$) channel. Sect. VI describes the procedure for the identification of secondary vertices from $b \rightarrow J/\psi$ decays and their separation from the prompt J/ψ background. In Sect. VII, independent confirmations of the b content of the selected events are provided. In Sect. VIII, the muon and electron data are combined into the final result, which is then compared with the existing experimental data on $\sigma(b\bar{b})$ and recent theoretical predictions. The main systematic uncertainties of the measurement are discussed. Sect. IX provides a brief summary of the analysis.

II. MEASUREMENT METHOD

The total $b\bar{b}$ production cross section in proton-nucleon (pN) interactions, integrated over the complete phase space, is the quantity of interest for characterizing the b production rate since it is most readily compared to theoretical calculations and other experimental results. However, in fixed-target experiments, the proton-nucleus (pA) cross section is measured for the actual detector acceptance ($\Delta\sigma_{b\bar{b}}^A$) and then 1) scaled to the proton-nucleon cross section taking into account the known (or assumed) nuclear dependence and 2) extrapolated to the full phase space by using theoretical models or information from other experiments.

In the present analysis, systematic uncertainties related to detector and trigger efficiencies are minimized by measuring the $b\bar{b}$ cross section relative to the J/ψ cross section in the kinematic region in our acceptance. The analysis consists essentially of two steps: 1) the J/ψ selection to determine the number (n_P) of prompt J/ψ mesons (Sect. V) which are copiously produced on the target; 2) the selection and counting of J/ψ mesons detached from the primary interaction vertex (Sect. VI), originating from $b \rightarrow J/\psi$ decays ($n_{b\bar{b}}$). Following this strategy, the ratio of $b\bar{b}$ to prompt J/ψ production cross sections in our acceptance ($\Delta\sigma_{b\bar{b}}^A/\Delta\sigma_P^A$) can be written as

$$\frac{\Delta\sigma_{b\bar{b}}^A}{\Delta\sigma_P^A} = \frac{n_{b\bar{b}}}{n_P} \cdot \frac{1}{\varepsilon_R \cdot \varepsilon_{b\bar{b}}^{\Delta z} \cdot \text{Br}(b\bar{b} \rightarrow J/\psi X)}, \quad (1)$$

with $\varepsilon_R = \varepsilon_{b\bar{b}}^{J/\psi}/\varepsilon_P^{J/\psi}$, where $\varepsilon_{b\bar{b}}^{J/\psi}$ and $\varepsilon_P^{J/\psi}$ are the detection efficiencies (including trigger, reconstruction and selection) for J/ψ from b decays and prompt J/ψ , respectively. $\varepsilon_{b\bar{b}}^{\Delta z}$ is the detached vertex selection efficiency. $\text{Br}(b\bar{b} \rightarrow J/\psi X) = 2 \cdot (1.16 \pm 0.10)\%$ [11] is the inclusive $b\bar{b} \rightarrow J/\psi X$ branching ratio, assumed to be the same in hadroproduction as that measured in Z decays.

All the quantities entering into Eq. (1) (except the branching ratio) are evaluated for J/ψ mesons produced in the kinematic range covered by HERA-B. In terms of Feynman- x (x_F) and transverse momentum (p_T), the kinematic range covers the intervals $-0.35 < x_F < 0.15$ and $0 < p_T < 6$ GeV/c. This will be indicated in the following as the HERA-B acceptance range.

The prompt J/ψ cross section (σ_P^A) has been measured at various energies ($\sqrt{s} \in [10, 200]$ GeV) and using various target materials ($A \in [1, 197]$) both in fixed target and collider experiments. σ_P^A is usually expressed by parameterizing the atomic weight (A) dependence of the cross section as $\sigma_P^A = \sigma_{J/\psi} \cdot A^\alpha$, where $\sigma_{J/\psi}$ is the J/ψ production cross section for proton-nucleon interactions and α has been measured with high statistical precision as a function of x_F and p_T by the E866 collaboration [12] providing an average value of $\alpha = 0.96 \pm 0.01$ in our x_F range.

The actual value of $\sigma_{J/\psi}$ is needed to obtain the absolute $\sigma(b\bar{b})$ cross section and it is known [1] that the values at energies around $\sqrt{s} = 20-50$ GeV scatter strongly. To determine the value of $\sigma_{J/\psi}$ at the HERA-B energy, a global analysis [13] has been performed on all published J/ψ cross section measurements¹. The best value, obtained from a fit on $\sigma_{J/\psi}(\sqrt{s})$ data with the help of a NRQCD model evaluated at the next-to-leading order is $\sigma_{J/\psi}(41.6 \text{ GeV}) = (502 \pm 44)$ nb/nucleon. The main uncertainty is systematic and has been evaluated by changing the selection of data submitted to the fit and by changing the free parameters in the model. Taking into account that the fraction of prompt J/ψ mesons produced in the HERA-B acceptance range is $f_P = (83 \pm 1)\%$ (see Sect. IV), we will assume a reference prompt J/ψ cross section in our acceptance which is given by: $\Delta\sigma_{J/\psi} = f_P \times \sigma_{J/\psi} = (417 \pm 37)$ nb/nucleon.

The A dependence of the $\sigma_{b\bar{b}}^A$ cross section has not been measured. In this paper, we assume the form $\sigma_{b\bar{b}}^A = \sigma(b\bar{b}) \cdot A^{\alpha_b}$, with $\alpha_b = 1$ since no nuclear suppression is expected in open bottom or open charm hadroproduction [15]. This expectation is confirmed in D -meson production data [16]. The same assumption is made in all published fixed-target $\sigma(b\bar{b})$ measurements.

The different A dependences of prompt J/ψ and $b\bar{b}$ cross sections complicate the evaluation of the cross section ratio when combining data sets from different target materials and several approaches are possible. Since in the present case $n_{b\bar{b}}$ suffers from low statistics in some sub-samples, we express the $b\bar{b}$ to J/ψ cross section ratio per nucleon in our acceptance range ($R_{\Delta\sigma}$) as:

$$R_{\Delta\sigma} = \frac{\Delta\sigma(b\bar{b})}{\Delta\sigma_{J/\psi}} = \frac{n_{b\bar{b}}}{\text{Br}(b\bar{b} \rightarrow J/\psi X) \cdot \sum_i n_P^i \cdot \varepsilon_{R,i} \cdot \varepsilon_{b\bar{b},i}^{\Delta z} \cdot A_i^{\alpha_b - \alpha}}, \quad (2)$$

where $n_{b\bar{b}}$ is the total number of detached J/ψ events found in the acceptance, n_P^i , $\varepsilon_{R,i}$ and $\varepsilon_{b\bar{b},i}^{\Delta z}$ are respectively the numbers of prompt J/ψ , the J/ψ selection efficiency ratios and the detached vertex selection

¹ The global fit includes our own measurement of the J/ψ cross section ($663 \pm 74 \pm 46$ nb/nucleon [14]). We prefer to normalize the present measurement to the value given by the global fit since the fit provides a complete summary of all available measurements.

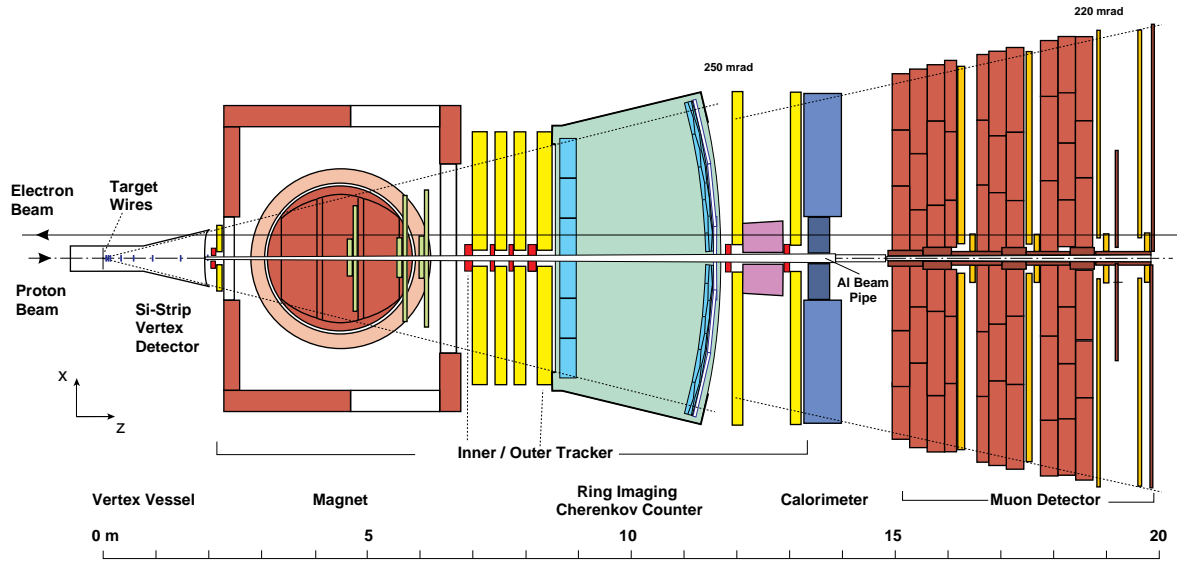


FIG. 1: Plan view of the HERA-B detector.

efficiencies measured on the sub-sample i taken with a target of atomic weight A_i . The quantity defined by Eq. (2) has the advantage of minimizing the dependence on theoretical models and on extrapolations. We also quote the $b\bar{b}$ cross section for full phase space, evaluated as $\sigma(b\bar{b}) = R_{\Delta\sigma} \cdot \Delta\sigma_{J/\psi}/f_{b\bar{b}}$, where $f_{b\bar{b}}$ is the fraction of J/ψ mesons from b decays in the HERA-B acceptance range. The quantity $f_{b\bar{b}}$ is determined through theoretical models as discussed in Sect. IV.

III. DETECTOR, TRIGGER AND DATA SAMPLE

HERA-B [17, 18] is a fixed target experiment at the HERA storage ring at DESY. The spectrometer and the trigger system were designed for efficient real-time filtering of b hadrons based on an online reconstruction of J/ψ mesons.

A. Detector

The spectrometer (Fig. 1) has a forward geometry, covering from 15 to 220 mrad in the bending plane, and from 15 to 160 mrad vertically. The detector features high resolution tracking and vertex reconstruction, good particle identification over a large momentum range, and a multilevel dilepton trigger.

The wire target [19] consists of two independent stations containing 4 wires each and separated by 40 mm along the beam direction. The wires are made of various materials (C, Al, Ti, Pd, W) with dimensions of 50–100 μm perpendicular to the beam and 50–500 μm along the beam. Up to eight target wires can be operated simultaneously and each wire can be moved independently into the proton beam halo to adjust the interaction rate. During the data taking, the target operated at rates of about 7 MHz, both in single and double wire configurations.

The Vertex Detector System (VDS) [20], located downstream of the target, consists of 8 planar stations with a total of 64 silicon microstrip detectors ($\approx 50\mu\text{m}$ readout pitch). It provides high spatial resolution for the reconstruction of primary and secondary vertices. A resolution of about 450 μm on J/ψ decay vertices along the direction of flight was achieved, fulfilling design specifications.

The main tracking system is located behind a 2.13 T·m bending magnet and extends to 13 m downstream of the interaction region. The granularity of the tracking system was adapted to the increasing particle density with decreasing distance to the beam. The Inner TRacker (ITR) [21] covers the range up to 20 mrad with Micro Strip Gas Chambers (MSGC) equipped with GEM foils. The Outer TRacker (OTR) [22], made of honeycomb drift chambers, reached a hit resolution of about 350 μm . The overall tracking system, consisting of VDS, OTR and ITR, reached a muon momentum resolution of $\Delta p/p(\%) = (1.61 \pm 0.02) \oplus (0.0051 \pm 0.0006)p$ where the momentum p is in GeV/c and in the range $5 < p < 80 \text{ GeV}/c$.

Particle identification is performed by a Ring Imaging Cherenkov detector (RICH), an Electromagnetic CALorimeter (ECAL) and a MUON system.

The RICH detector [23] provides pion–kaon–proton separation. It uses a 2.5 m long C_4F_{10} radiator volume for Cherenkov light emission by charged particles, which after reflection in spherical and planar mirrors, is directed to one of two planes of photomultiplier tubes.

The ECAL [24] is optimized for good electron/gamma energy resolution and electron-hadron discrimination. It is composed of 5956 independent calorimeter modules built with shashlik technology. The cell size increases with the distance from the beam. The detector is instrumented with a fast digital readout and a pretrigger system which provides reconstructed clusters with large transverse energy (pretrigger seeds). The energy resolutions for the three ECAL regions (Inner, Middle, Outer) are, respectively, $\sigma_E/E = 20.5\%/\sqrt{E} \oplus 1.2\%$, $\sigma_E/E = 11.8\%/\sqrt{E} \oplus 1.4\%$ and $\sigma_E/E = 10.8\%/\sqrt{E} \oplus 1.0\%$ [25]. Spatial resolutions, determined with π^0 decays, are ranging from 1 to 8 mm depending on the ECAL region and the particle energy.

The MUON system [26] consists of four tracking stations located in the most downstream part of the detector at various depths in an iron and concrete muon–absorber. The active elements are mainly conventional tube chambers arranged in double layers. Pad cathodes coupled to the tubes of the two most downstream tracking stations are used for pre-triggering purposes.

B. Trigger Configuration

The dilepton trigger is initiated by pretrigger (PT) signals from either the MUON system [27] or the ECAL [28]. Dual pad coincidences in the MUON system or complete ECAL clusters with a transverse energy above 1 GeV constitute the basic trigger seeds. These are used by the First Level Trigger (FLT) [29] to define a sequence of regions of interest inside the OTR, which are used to initiate a search for track candidates originating from J/ψ decays. Track parameters as well as the PT seeds are then sent to the Second Level Trigger (SLT) [30], which is a highly configurable software filter that extrapolates found tracks through the magnet and VDS, finally applying a mild vertex constraint.

More specifically, for the data presented here, the FLT required the presence of at least two PT seeds and at least one reconstructed track originating from one of the PT seeds. The SLT searched for tracks starting from the PT seeds, requiring that at least two complete tracks, with segments in the OTR and the VDS, be found and that the two tracks be consistent with a common vertex hypothesis. Moreover, the SLT track-seeding algorithm imposed a target constraint by including in the initial track parameters a point near the center of the active target wires with uncertainties large enough to accommodate tracks from all targets and also to allow for the finite B lifetime. Accepted events were read out and sent to an online reconstruction farm [31].

The J/ψ trigger worked constantly at rejection factors around 4×10^4 , matching the typical data recording rate of 120 Hz (to tape). The experiment routinely achieved an event yield of about 1200 J/ψ mesons per hour at an interaction rate of about 7 MHz.

C. Data Sample

The data sample used in this analysis was collected between October 2002 and March 2003. During this period, 164 million dilepton-triggered events were recorded containing about 300,000 J/ψ mesons. These are distributed almost equally between the dimuon and dielectron channels.

Data were taken in nine different wire configurations of single or double wire runs, for a total of 14 equivalent single-wire samples. The wire materials used were carbon ($A=12$, $\approx 64\%$ of the J/ψ sample), tungsten ($A=184$, $\approx 27\%$), and titanium ($A=48$, $\approx 9\%$).

During the data taking period, the detector was operated under constant monitoring. The data quality was assessed both online and offline. Only runs with good performance of all the main detector components and stable trigger conditions are used. Five periods with constant experimental conditions were defined and the data were grouped accordingly.

IV. MONTE CARLO SIMULATION

Monte Carlo (MC) simulations are used to determine the efficiency terms entering into the cross section equation (Eq. 2), to determine the criteria to select the $b \rightarrow J/\psi$ candidates, and to understand the nature of the background. The simulation includes our best knowledge of the physics of the processes under investigation, of the detector, of the trigger and of the event reconstruction.

To best describe interactions in the HERA-B environment, the Monte Carlo generator exploits a combination of features of different standard tools. The simulation of heavy quark (Q) production is obtained by generating the basic process $pN \rightarrow Q\bar{Q}X$ with PYTHIA 5.7 [32] and hadronizing the heavy quarks using the JETSET 7.4 [32] package. In the second step, the remaining energy and momentum of the collision is used by FRITIOF 7.02 [33] to provide the underlying inelastic event and to generate further interactions inside the target nucleus. After these steps, the generated particles are passed through the GEANT 3.21 package [34] for detector simulation.

For an accurate description of the kinematic characteristics of prompt J/ψ production, experimental data on prompt J/ψ differential cross sections $d\sigma/d(p_T^2)$ and $d\sigma/dx_F$ [35] are used to tune the standard generator: all the produced events are weighted to match the available proton-silicon measurements on differential J/ψ cross sections. Since these are available in the positive x_F region only, we assume a symmetric x_F distribution of prompt J/ψ production: $d\sigma/dx_F = \beta \cdot (1 - |x_F|)^c$ where $c = 6.38 \pm 0.24$ [35]. This extension conforms both to all the basic charmonium production models and to our own data on the J/ψ differential cross sections [36]. The model dependence of the generated p_T spectrum is of minor importance since the acceptance for the J/ψ p_T is essentially flat. The influence of a possible J/ψ polarization within the limits given by experimental results [35, 37] is taken into account in the systematic uncertainties of the prompt J/ψ MC. With this model, the fraction f_p of prompt J/ψ mesons produced in the HERA-B acceptance range is $f_p = (83 \pm 1)\%$, where the error is due to the uncertainty in the exponent c of the proton-silicon data fit [35].

Since, for open b production, there are no measured differential cross sections, we use a $b\bar{b}$ production model which is mostly based on NRQCD theory [38]. As in the case of charmonium production, the PYTHIA generated $b\bar{b}$ events are weighted with a model containing several contributions: 1) the generated b quark kinematics (x_F and p_T), as given by the computation of Mangano *et al.*, using the most recent next-to-leading-order MRST parton distribution function [39] with a b quark mass of $m_b = 4.75 \text{ GeV}/c^2$ and a QCD renormalization scale $\mu = \sqrt{m_b^2 + p_T^2}$; 2) the intrinsic transverse momenta of the colliding quarks, smeared with a Gaussian distribution resulting in $\langle k_T^2 \rangle = 0.5 \text{ GeV}^2/c^2$ [40]; and 3) the b fragmentation function, described by a Peterson shape [41] with a parameter $\epsilon = 0.006$ [42]. The subsequent b hadron formation and decay are described by the PYTHIA default parameters. Possible b hadron polarization and J/ψ polarization in b decays are assumed to be null. With these assumptions, the fraction of detached J/ψ mesons produced in the HERA-B acceptance range (see Sect. II) is $f_{b\bar{b}} = (90.6 \pm 0.5)\%$, where the error is determined in the systematic studies described below.

The sensitivity of the measured cross section ratio $R_{\Delta\sigma}$ to the $b\bar{b}$ MC model parameters has been determined by varying: the parton distribution functions (from MRST to CTEQ5 [43]), the b quark mass (in the range $m_b \in [4.5, 5.0] \text{ GeV}/c^2$), the QCD renormalization scale (from $0.5\sqrt{m_b^2 + p_T^2}$ to $2\sqrt{m_b^2 + p_T^2}$), the fragmentation function (from the Peterson form [8, 42, 44] with parameter $\epsilon \in [0.002, 0.008]$, to the Kartvelishvili form [45] with parameter $\alpha_\beta = 13.7 \pm 1.3$ [44]), the intrinsic transverse momentum distribution (with $\langle k_T^2 \rangle$ in the range $[0.125, 2.0] \text{ GeV}^2/c^2$) and the fraction of b baryons produced in the b hadronization process in the range $[0, 12]\%$. The observed variations in the detection efficiencies have been included in the systematic uncertainty. No significant dependence ($< 1.5\%$) of the cross section ratio has been found on the momentum of the J/ψ mesons in the b hadron rest frame nor on the polarization of J/ψ mesons coming from b decays.

The GEANT tracking step is performed with the help of a detailed description of the detector which includes both the active (instrumented) and inactive (support structure) elements. The detector response is simulated by reproducing the digitization of electronic signals and of the read-out chain. A status (masked/dead/alive) and an efficiency is associated to each channel to take into account the measured efficiency in data as well as the faulty/noisy/masked channels. This information was produced for each data-taking sub-period (see Sect. III C). The MC events are subjected to a full trigger simulation and reconstructed with the same code as the data. For each data sub-sample, MC samples were produced for the signal channels and background sources to evaluate the efficiency terms in Eq. (2) for the specific running conditions.

V. J/ψ EVENT SELECTION

The first stage of the analysis is devoted to the determination of the number of J/ψ mesons produced at the target, which is dominated by the prompt production. This is done in several steps: selection of well-measured tracks, lepton identification, lepton pair selection and J/ψ candidate counting. Most of the selection criteria are common for the muon and the electron final states and are described first. Other details specific to the different lepton types (for example, particle identification and counting of prompt candidates) are discussed separately.

The cuts applied for prompt J/ψ signal selection mostly reflect the detector acceptance and requirements already explicitly or implicitly imposed by the trigger algorithms. Therefore the lepton track search initially uses information provided by the trigger. The parameters of the SLT track candidates that resulted in a trigger decision are given as seeds to the offline reconstruction program. If a seed successfully results in a reconstructed track, it is flagged as a ‘trigger track’. Only these are considered in the search for J/ψ candidates.

Further selection is performed on the offline reconstructed tracks, which profit from improved reconstruction due to more accurate calibration and alignment constants compared to those used online. Basic cuts on the number of hits in the VDS and in the main tracker (OTR+ITR), and on the χ^2 probability of the track fit are used to select only well-reconstructed tracks and to reject mismeasured and ghost tracks. Weak cuts on momentum ($6.0 < p < 200$ GeV/ c) and transverse momentum ($0.7 < p_T < 5.0$ GeV/ c) are applied. The lower cuts mostly reflect the detector acceptance and the trigger requirements. In the muon case, they also improve the rejection of hadrons traversing the absorber and of muons from π/K decays in flight. The upper cuts discard tracks with momenta above the expected range for J/ψ decay products.

To complete the single lepton selection, requirements on the relevant particle identification specific to muon or electron channels are imposed and are discussed separately in Sect. V A and V B.

When two lepton candidates with opposite charge are selected, a vertex fit is performed. Only dilepton candidates with a χ^2 probability greater than 1% are considered further. This requirement ensures that the tracks originate from the same vertex and helps to reject combinatorial background and background from $c\bar{c}$ and $b\bar{b}$ double semileptonic decays in the subsequent detached vertex analysis. Moreover, the dilepton x_F is required to be between -0.35 and 0.15 to match the detector acceptance. Only one dilepton candidate per event is accepted. When more than one dilepton candidate survives all cuts, the one with the best particle identification for both leptons is chosen.

A. $J/\psi \rightarrow \mu^+ \mu^-$

The identification of muon tracks is simplified by the fact that only muons have a significant probability of penetrating through the absorbers of the MUON detector. Therefore a minimal set of cuts on signals from this detector (hit multiplicity and muon likelihood \mathcal{L}_μ) is sufficient for robust muon identification. In case more than one muon pair is selected, the pair with the highest product of muon likelihoods is chosen.

The dimuon mass spectrum obtained with this selection is shown in Fig. 2a. The number of prompt J/ψ candidates is determined by fitting the mass distribution to a function derived mainly from Monte Carlo studies [46]. This function includes: 1) a description of the non-Gaussian shape of the J/ψ signal², 2) a radiative tail due to the $J/\psi \rightarrow \mu^+ \mu^- \gamma$ decay, 3) a Gaussian shape for the $\psi(2S)$ signal and 4) an exponential function for the background.

The mean value of the J/ψ mass is $3093.5 \pm 0.2_{\text{stat}}$ MeV/ c^2 , and the full width at half maximum (FWHM) of the background subtracted J/ψ peak is 90 MeV/ c^2 . The shift observed in the J/ψ mass with respect to the PDG value [11] is due to small systematic effects in the tracking and in the internal alignment of the detector. The total number of reconstructed J/ψ mesons is $n_P(\mu^+ \mu^-) = 148200 \pm 500$. This number depends slightly on the fitting function and mass interval considered. These uncertainties are included in the systematic error (Sect. VIII).

² A symmetric function composed of three Gaussians is used, to take properly into account the details of the momentum resolution in a complex apparatus such as HERA-B.

B. $J/\psi \rightarrow e^+e^-$

The electron and positron selection is affected by larger background contributions than the muon case, mostly due to pions interacting in the ECAL and hadrons overlapping with energetic neutral showers. Requirements on the lepton identification are therefore more demanding than in the muon case. Additional corrections are used to improve the accuracy of the electron momentum estimate.

The electron track candidates are selected by requiring an ECAL cluster with a transverse energy greater than 1.0 GeV, matched to the track, both at the trigger and the offline analysis levels. In the non-bending direction (y), the distance Δy between the track position extrapolated to the ECAL and the reconstructed ECAL cluster must satisfy the requirement $|\Delta y/\sigma_{\Delta y}| < 3.0$, where $\sigma_{\Delta y}$ is the resolution on Δy for clusters and tracks from e^\pm . The typical resolutions are in the range 3–10 mm depending on the ECAL region. Cluster-track matches from random combinations and from hadron interactions in the calorimeter are substantially suppressed by this cut since their Δy distributions are wider by more than a factor two compared to e^\pm tracks.

For a precise measurement of the electron momentum, some corrections to the value provided by the tracking system are needed. During their passage through the material in front of the ECAL, electrons can emit bremsstrahlung (BR) photons and lose energy due to ionization processes. ECAL clusters due to BR photons emitted before the magnet are searched for in the ECAL at a location given by the extrapolation of the initial track direction to the ECAL position. If a BR cluster with a measured energy $E_{\text{BR}} > 1$ GeV is found, the energy of the cluster is added to the electron momentum at the production point. The correction ($\approx 1 - 2\%$) for further energy losses is evaluated stochastically via Monte Carlo simulations.

Electron identification in the ECAL is mainly based on the ratio of the cluster energy (E) to the momentum obtained from the tracking (p). Typical E/p distributions for e^\pm signals have a Gaussian shape with mean 0.99 and width $\sigma \approx 6\%$. Since the requirement on E/p is also crucial in the selection of the detached signal, it was included in the optimization procedure described in Sect. VI. The obtained cut values are $-2.0\sigma < E/p - 0.99 < 3.5\sigma$. If more than one electron-positron pair is found in one event, the combination with the best E/p ratio is taken.

Requiring that at least one of the electrons from a J/ψ candidate has an associated bremsstrahlung photon (BR tag) or that both leptons have BR tags increases the signal-to-background ratio from 0.6 to 3 and 9, respectively, providing a powerful method to isolate clean samples. These are used for studies of resolutions (for example, of Δy and E/p) and for cross checks. As explained in [10], the probability that a BR photon is emitted and detected in a separated ECAL cluster (bremsstrahlung tag probability) can be measured redundantly by counting J/ψ mesons for different tag criteria. For the current setup, the average tag efficiency (ε_{BR}) is $\varepsilon_{\text{BR}} = 0.30 \pm 0.01_{\text{stat}} \pm 0.01_{\text{sys}}$ per track. The same analysis, performed on MC events, yields a MC tag probability of $\varepsilon_{\text{BR}}^{\text{MC}} = 0.29 \pm 0.01_{\text{stat}} \pm 0.01_{\text{sys}}$, in agreement with data. This gives further confidence in the quality of our detector description and MC simulation, in particular in the crucial region in front of the magnet, where the triggered electrons cross about 0.07 radiation lengths of material.

The BR tag played a central role in the previous analysis [10], since it was used for counting the number of prompt J/ψ candidates. Subsequent improvements in ECAL stability and removal of material in the magnet region resulted in reduced combinatoric background and better mass resolution. Consequently the BR tag is now only used for calibration and cross-checks and not for signal counting.

The invariant mass spectrum obtained for the final $J/\psi \rightarrow e^+e^-$ sample is shown in Fig. 2b. As for the muon case, the number of prompt J/ψ candidates is determined by fitting the mass distribution with a function determined from MC studies. It includes 1) Gaussian functions for the J/ψ and for the $\psi(2S)$ signal, 2) a function to take into account the radiative tail of the charmonium decays and 3) an exponential-like function for the background. The radiative tail contains both the partially reconstructed $J/\psi \rightarrow e^+e^-\gamma$ decays as well as the tail due to incomplete electron energy measurement or BR recovery. The mean value of the J/ψ mass is $3109 \pm 1_{\text{stat}}$ MeV/ c^2 , and the FWHM of the background subtracted J/ψ peak is 140 MeV/ c^2 . The total number of $J/\psi \rightarrow e^+e^-$ candidates is $n_P(e^+e^-) = 103800 \pm 1000$.

VI. DETACHED VERTEX ANALYSIS

In the second stage of the analysis, J/ψ mesons produced in the decay of a b hadron are searched for. The mean decay length of a b hadron in the HERA-B acceptance is about 8 mm. Accordingly, the J/ψ mesons produced in b decays are typically well-detached from the primary interaction at the target wires. The $b \rightarrow J/\psi$ candidate selection is performed in two tightly correlated steps: first, a J/ψ candidate (as described in the previous section) is assigned to one target wire and to one primary interaction vertex. Then,

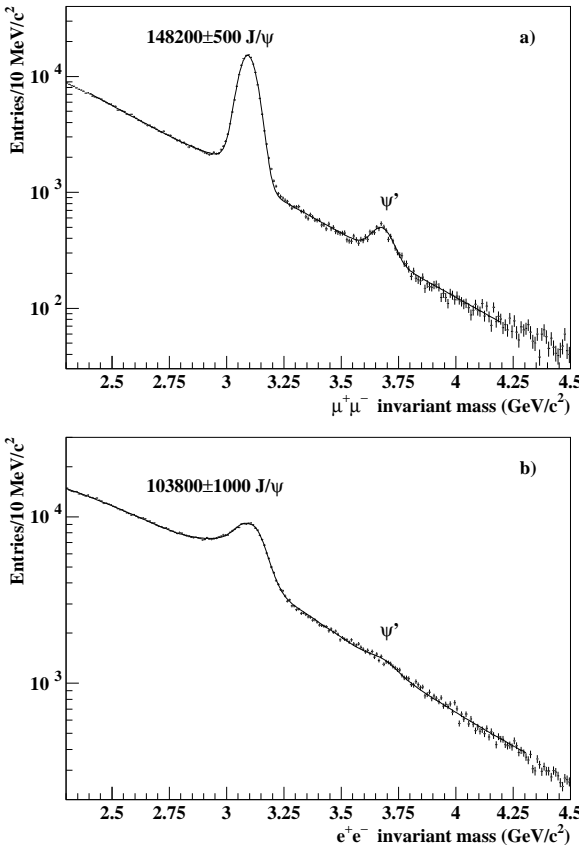


FIG. 2: Invariant mass plots for both J/ψ -decay channels: a) muon sample, b) electron sample.

if the association is unambiguous, cuts designed to distinguish J/ψ mesons coming from b decays from those produced promptly at the target are applied. Almost all cuts are applied on the significance of the relevant quantity (ratio of a quantity to its uncertainty) rather than on its unnormalized value, to take advantage of the error information. The variables used to isolate detached J/ψ mesons are described in the following.

The decay length is defined as the distance between the primary interaction point and the J/ψ vertex along the proton beam direction (which defines the HERA-B z axis). The positions of target wires, averaged over many consecutive events, define better the primary interaction point than the fitted positions of individual primary vertices; therefore the decay length is calculated with respect to the target wire. With a dilepton vertex resolution of about $450\ \mu\text{m}$ in z , the decays of b hadrons can be separated from primary vertices with high efficiency.

For J/ψ mesons produced at a detached vertex, each of the decay leptons is likely to be inconsistent with being produced at the target. Therefore a cut on their impact parameters to the wire, defined as the lepton distance from the wire at the z -coordinate of the wire, is applied. This requirement is very effective for reducing background, as the wire position is known in two dimensions with high precision.

On the other hand, since the direction of the produced J/ψ meson is nearly collinear with that of the b hadron, the impact parameter of the J/ψ to the wire is typically small (mostly below $20\ \mu\text{m}$). An upper cut is applied to remove combinatorial background, as well as background from semileptonic $b\bar{b}$ and double semileptonic $c\bar{c}$ decays.

For double wire runs and for multiple primary vertex events, the quantities described above can only be defined after association of the dilepton candidate to the correct target wire and to the correct primary interaction vertex. For this purpose, we define two χ^2 -like quantities based on the lepton and the dilepton impact parameters to a wire and on their distances of closest approach to a primary vertex. The wire and the vertex for which the corresponding χ^2 is minimum are associated to the dilepton candidate. Events in which the wire of the dilepton and the wire of the associated primary vertex do not match are discarded. In this way, the probability for wrong wire assignment, estimated from $b\bar{b}$ MC events, is less than 1%.

Moreover, in the case of double wire runs, it is possible that a lepton candidate from an interaction on one

wire is combined with a lepton candidate originating from the other wire. Since the reconstructed vertex of these two leptons tends to lie between the two wires, these events are a dangerous source of background for the detached signal. To reduce this type of background, events in which one or both leptons are pointing to a reconstructed primary vertex on a different wire than the assigned one are discarded.

Events having unambiguous wire-vertex association are analyzed further. We exclude events with the absolute value of the decay length $|\Delta z| < 2$ mm (fiducial volume cut), in order to ensure that the J/ψ vertex is well outside of the target wire. This removes more than 99% of prompt J/ψ background while keeping more than 75% of the signal. Afterwards, on the total sample a cut optimization procedure is applied, on the following quantities: the Δz significance, the lepton and the dilepton impact parameters to the wire and the lepton and dilepton distances of closest approach to the primary vertex and E/p for electrons.

A. Cut Optimization Procedure

To avoid biasing our signal yield and resulting cross section ratio, we choose our selection criteria 'blindly', i.e. without looking at events in the signal region until all selection criteria are finalized. The quantity to be maximized as a function of the cuts is the signal significance $S/\sqrt{S + BG}$ in a fixed dilepton invariant mass window, where the signal (S) is taken from $b \rightarrow J/\psi$ MC events, and the background (BG) is obtained by combining MC and real data. The main background sources are listed below. The first three contributions are estimated from MC, the fourth from data:

- A possible prompt J/ψ background surviving detachment cuts is one of our main concerns, since there is no way to distinguish it from J/ψ mesons coming from b decays. Its yield is proportional to the prompt J/ψ cross section. A large MC sample ($\approx 10^7$ events) is used to estimate the surviving background contribution.
- A large fraction of the background is coming from $b\bar{b}$ events where both b quarks produce a high- p_T lepton. The yield of this background is proportional to the $b\bar{b}$ cross section.
- Double semileptonic $c\bar{c}$ decays can contribute in a similar way. The intrinsic p_T cut at the trigger level removes most of this background. Nevertheless this contribution cannot be neglected, since the cross section for $c\bar{c}$ events is larger than the $b\bar{b}$ cross section by three orders of magnitude.
- Another contribution is due to combinatorial background, i.e. dileptons made of incorrectly reconstructed or fake tracks, or tracks coming from kaon or pion decays in flight. Its size can be estimated from the number of events in which the dilepton vertex is reconstructed in the unphysical region upstream of the target. Also, like-sign lepton pairs (available only for the muon channel) or dileptons artificially formed by tracks from different events can give an estimate of this background.

The background used for the cut optimization is an appropriately scaled combination of prompt J/ψ MC, $b\bar{b}$ and $c\bar{c}$ double semileptonic MC events and either like-sign data events (in the muon channel) or upstream data events for the combinatorial background. The relative contribution of the different samples is estimated on the basis of the relative cross sections (for the MC samples) and from the upstream spectrum for the combinatorial background. Since the $b\bar{b}$ cross section is not known (being the goal of the current measurement), its value is left to vary in a range between a quarter and double of our previous measurement [10]. The optimization is repeated for several intermediate values. A stability check is also performed by varying the initial values of the cuts in order to verify the independence of the minimization results on the initial conditions.

This approach can work effectively only if the data distributions are well reproduced by MC. This is verified for all the quantities used for the selections. As an example, in Fig. 3, the distributions of the lepton impact parameter to the wire are shown for a sample of background subtracted $J/\psi \rightarrow \mu^+\mu^-$ (a) and a sample of background subtracted double bremsstrahlung tagged $J/\psi \rightarrow e^+e^-$ (b). Agreement between data and MC is obtained for all variables used in the optimization procedure for both channels.

Of the six parameters entering in the optimization procedure, the cuts on the lepton's and dilepton's closest distance of approach to the primary vertex are fixed by the optimization procedure to a value where all events surviving the other cuts are selected. Therefore these cuts have been removed from the optimization procedure and will not be mentioned further.

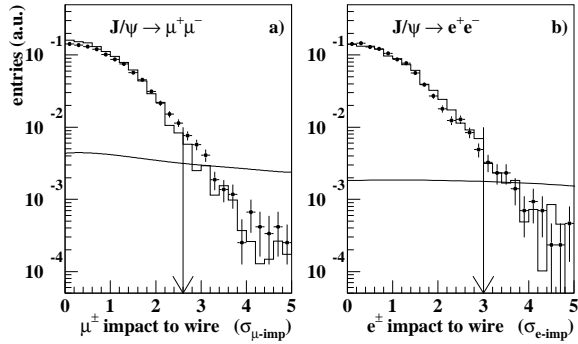


FIG. 3: Comparison between the distribution of the lepton impact parameter to the wire for real data (points with error bars) and for the prompt J/ψ MC (histogram). a) $J/\psi \rightarrow \mu^+\mu^-$ candidates selected in the region $2.95 < m_{\mu^+\mu^-} < 3.25$ GeV/c^2 after sideband subtraction for real data, b) double BR tagged $J/\psi \rightarrow e^+e^-$ candidates selected in the region $2.9 < m_{e^+e^-} < 3.2$ GeV/c^2 after sideband subtraction for real data. The continuous solid line shows the $b \rightarrow J/\psi$ MC sample (arbitrary normalization) while the arrows mark the cut position determined by the optimization procedure.

B. $b \rightarrow J/\psi X \rightarrow \mu^+\mu^- X$

The cut values obtained with the optimization procedure for the muon channel are listed in the second column of Table I. Once the cuts are applied, only 268 events with secondary vertices downstream of the primary interactions and having a dilepton invariant mass above 2.2 GeV/c^2 survive, while upstream of the target (unphysical region for $b \rightarrow J/\psi$ decays), 33 events are found in the same mass region. The invariant mass distribution of these detached candidates is shown in Fig. 4, where a clear peak corresponding to the J/ψ mass is present only in the downstream sample.

Cut	$\mu^+\mu^-$ value	e^+e^- value	Optimized
Absolute Δz	> 2 mm	> 2 mm	no
Δz significance	$> 9.0 \sigma$	$> 10.0 \sigma$	yes
Lepton impact to wire	$> 2.6 \sigma$	$> 3.0 \sigma$	yes
J/ψ impact to wire	$< 9.0 \sigma$	$< 12.0 \sigma$	yes
Lepton identification	$\mathcal{L}_\mu > 0.05$	$-2.0 \sigma < E/p - 0.99 < 3.5 \sigma$	E/p only

TABLE I: Cut values used to select the detached J/ψ candidates in the muon and in the electron channels. Quantities submitted to the blind optimization procedure are explicitly indicated in the last column.

To count the detached J/ψ candidates, an unbinned maximum likelihood fit is performed using the reconstructed invariant mass values. In the fit, the function used for the prompt J/ψ analysis models the peak and an exponential function models the background. As free fit parameters, we use the J/ψ and background yields and the slope of the exponential. When the mass position and width of the peak are left as free parameters, the obtained values are consistent with those of the prompt J/ψ spectrum. Thus, the final results are given with the mass and width fixed to the values of the prompt signal. In Fig. 4b, the solid line shows the result of the likelihood fit. For the fit to the total data sample, we find $n_{b\bar{b}} = 46.2^{+8.6}_{-7.9}$ and $n_{\text{bkg}} = 222 \pm 15$ events for the signal and the background, respectively, and a background slope parameter of $\lambda = -1.9 \pm 0.1$ (GeV/c^2) $^{-1}$.

As a cross check, a fit to the upstream events is performed with the same free parameters. In the full sample, the fit finds $n_{b\bar{b}} = -0.1 \pm 1.4$ J/ψ events, compatible with absence of signal, $n_{\text{bkg}} = 33 \pm 6$ background events and $\lambda = -1.9 \pm 0.3$ (GeV/c^2) $^{-1}$.

Using the like-sign spectrum and the background contributions surviving the optimization procedure, the final composition of the background in the detached dilepton spectrum has been estimated. Within statistical uncertainty, all the background can be accounted for by the four background sources described above, with

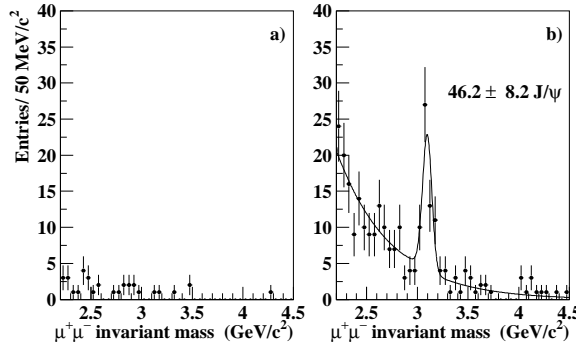


FIG. 4: Dimuon mass distributions after vertex detachment cuts, from the full muon sample. a) Upstream events (combinatorial background), b) downstream events. The solid line shows the result of the likelihood fit.

the dominant contributions being combinatorial (44%) and $b\bar{b}$ (43%) semileptonic decays. Since charm particles have a relatively short lifetime, their contribution to the background is suppressed (13%) by the detachment cuts. From MC, no prompt J/ψ event (< 0.7 at 90% C.L.) is expected to survive the detached vertex selection. Finally, in the region upstream of the target the background is purely combinatorial.

To determine $R_{\Delta\sigma}$ in our x_F range according to Eq. (2), the number of prompt J/ψ mesons and the efficiency terms must be evaluated for each of the 14 different sub-samples (one sample for each wire in each wire configuration, labelled i later). The number of prompt $J/\psi \rightarrow \mu^+\mu^-$ candidates in each sub-sample is evaluated with the procedure described in Sect. V A. To obtain the efficiencies, the MC events of prompt J/ψ and $b \rightarrow J/\psi$ are subjected to the same analysis chain used for the data. The average final value of the efficiencies is $\langle \varepsilon_{R,i} \cdot \varepsilon_{b\bar{b},i}^{\Delta z} \rangle = 0.400 \pm 0.006$, where the uncertainty is given by the statistical fluctuations and sub-sample variability only. All the results obtained for different target materials are summarized in Table II. The resulting value for $\frac{\Delta\sigma(b\bar{b})}{\Delta\sigma_{J/\psi}}$ in our kinematic range, averaged over all sub-samples and target materials, is:

$$R_{\Delta\sigma}(\mu^+\mu^-) = \frac{\Delta\sigma(b\bar{b})}{\Delta\sigma_{J/\psi}} = 0.0295 \pm 0.0055_{\text{stat}} \quad (3)$$

where the uncertainty is statistical only. The systematic uncertainties as well as the tests of the stability of the result are discussed in Sect. VIII.

C. $b \rightarrow J/\psi X \rightarrow e^+e^- X$

As discussed in Sect. V B, the $J/\psi \rightarrow e^+e^-$ decays are affected by a larger background and the selection of the detached vertex signal is therefore more critical. Since the electron particle identification (mainly based on the E/p ratio of the lepton tracks) is crucial for candidate selection, this quantity is included in the blind optimization procedure. The cut values obtained for the electron channel are listed in the third column of Table I. The Table shows that the optimized values for the cuts applied in the e^+e^- channel are close to those for the muon channel, albeit generally stronger. Only 229 events with dilepton vertices downstream of the primary interactions and with dilepton invariant masses above $2.0 \text{ GeV}/c^2$ survive these cuts, while 51 events with upstream dilepton vertices are found. The invariant mass distribution of these detached candidates is shown in Fig. 5; a peak is visible in the downstream sample at $m_{e^+e^-} = m_{J/\psi}$.

The same type of unbinned maximum likelihood fit used in the muon channel is performed also on the detached electron candidates, and the fit result is shown in Fig. 5b. For the total data sample, we find $n_{b\bar{b}} = 36.9^{+8.5}_{-7.8}$ and $n_{\text{bkg}} = 192 \pm 15$ events for the signal and the background, respectively, and a background slope parameter of $\lambda = -1.7 \pm 0.1 \text{ (GeV}/c^2)^{-1}$.

As a further cross check, a fit to the upstream events is performed with the same free parameters. The fit finds $n_{b\bar{b}} = -4.2 \pm 1.9$ signal events (compatible with absence of signal events), $n_{\text{bkg}} = 55 \pm 8$ background events and $\lambda = -1.6 \pm 0.2 \text{ (GeV}/c^2)^{-1}$.

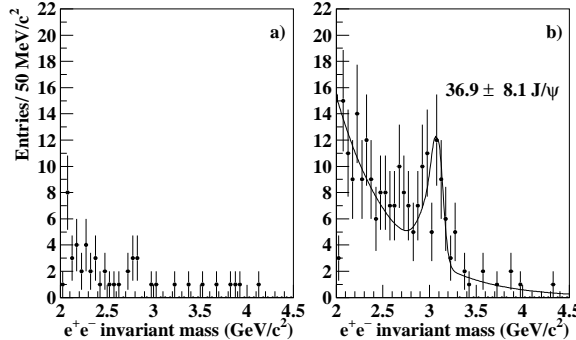


FIG. 5: Dilepton mass distribution after vertex detachment cuts, from the full electron sample. a) Upstream events (combinatorial background), b) downstream events. The solid line shows the result of the likelihood fit.

From the optimization procedure we can also extract the composition of the remaining background. As in the muon channel, the four sources considered can account for the obtained spectrum. The $b\bar{b}$ semileptonic decays are the dominant contribution (49%), followed by the combinatorial background (35%) and the open charm events (16%). Also, in this case no prompt J/ψ event (< 1.1 at 90% C.L.) is expected to survive the applied cuts for b selection.

As for the muon measurement, $R_{\Delta\sigma}$ is evaluated by determining the number of prompt J/ψ mesons and the efficiency terms separately for each sub-sample (Eq. 2). The average value of the efficiencies is $\langle \varepsilon_{R,i} \cdot \varepsilon_{b\bar{b},i}^{\Delta z} \rangle = 0.40 \pm 0.02$, which is close to that obtained in the muon analysis. The resulting value for $\frac{\Delta\sigma(b\bar{b})}{\Delta\sigma_{J/\psi}}$ in the electron channel in our kinematic range is:

$$R_{\Delta\sigma}(e^+e^-) = \frac{\Delta\sigma(b\bar{b})}{\Delta\sigma_{J/\psi}} = 0.0353 \pm 0.0078_{\text{stat}}, \quad (4)$$

in good agreement with the muon result (see Table II).

Channel	$\mu^+\mu^-$			e^+e^-		
Target	Carbon	Titanium	Tungsten	Carbon	Titanium	Tungsten
Atomic weight	12.01	47.87	183.84	12.01	47.87	183.84
Prompt J/ψ (n_P)	93700 ± 300	8080 ± 100	45560 ± 200	67100 ± 700	4800 ± 200	32400 ± 600
Detached J/ψ ($n_{b\bar{b}}$)	27.8 ± 6.3	3.0 ± 2.1	15.5 ± 4.8	$17.8^{+5.9}_{-5.2}$	0.9 ± 1.0	$18.4^{+6.2}_{-5.5}$
$\langle \varepsilon_{R,i} \cdot \varepsilon_{b\bar{b},i}^{\Delta z} \rangle$	0.398 ± 0.004	0.397 ± 0.011	0.404 ± 0.005	0.366 ± 0.007	0.424 ± 0.022	0.402 ± 0.014
α	0.96 ± 0.01			0.96 ± 0.01		
$\text{Br}(b\bar{b} \rightarrow J/\psi X)$	2.32 ± 0.20			2.32 ± 0.20		
$\Delta\sigma_{b\bar{b}}^A/\Delta\sigma_P^A (\times 10^{-2})$	3.22 ± 0.73	4.0 ± 2.8	3.6 ± 1.1	3.2 ± 1.0	1.8 ± 2.2	6.2 ± 2.0
$\Delta\sigma(b\bar{b})/\Delta\sigma_{J/\psi} (\times 10^{-2})$	2.95 ± 0.55			3.53 ± 0.78		

TABLE II: Quantities entering into the cross section ratio measurements for the two channels and for the three target materials. All the numbers are given for the x_F interval $[-0.35, +0.15]$.

VII. FURTHER b FLAVOR CONFIRMATION ANALYSES

To confirm the b flavor content of the selected detached vertex sample, several independent cross checks have been performed on it and on a second sample obtained by relaxing the selection cuts. The checks include an estimation of the mean lifetime of the detached candidates. Also a search is made for other decay products of the b hadrons in the enlarged selection, with the aim of a complete identification of exclusive decay channels or the identification of a potentially cleaner sample of three-prong detached vertices. These and other tests are described in the following.

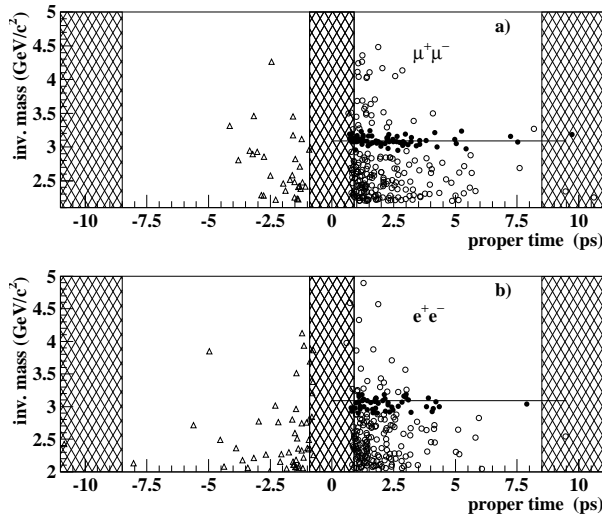


FIG. 6: Scatter plot of $\mu^+\mu^-$ (a) and e^+e^- (b) invariant mass versus the proper time for the detached candidates. The downstream detached candidates are marked with filled circles in the J/ψ regions ($3.0 < m_{\mu^+\mu^-} < 3.2$ GeV/c^2 and $2.9 < m_{e^+e^-} < 3.2$ GeV/c^2) and with open circles elsewhere. Upstream candidates are shown with open triangle marks. The hatches define the regions excluded from the mean lifetime measurement.

A. Lifetime Fit

The determination of the mean lifetime of the detached candidates is one of the clearest confirmations of the b flavor of the signal. A direct and precise measurement is however not possible, since in the inclusive $b \rightarrow J/\psi$ analysis the b hadron is not fully reconstructed and therefore its momentum and $\beta\gamma$ value are not known. However, MC studies show that a good estimator of the b hadron's $\beta\gamma$ is the corresponding value of the J/ψ meson produced in the decay. Because of this strong correlation, the proper time t_i of a b candidate can be approximated as $t_i = \Delta z_i / (\beta\gamma)_{J/\psi} \cdot k$, where Δz_i is the decay length, $(\beta\gamma)_{J/\psi}$ is the $\beta\gamma$ factor evaluated on the dilepton and k is a numerical factor (≈ 1.03) which corrects for the decay and trigger bias. Within the limits of this approximation, a mean lifetime measurement is therefore possible even without exclusive identification of b hadrons.

In Fig. 6, the scatter plots of the dilepton invariant mass versus the proper time for the muon and the electron candidates are shown. As can be seen, the proper time distribution behaves differently depending on the invariant mass region. To quantify these differences, unbinned maximum likelihood fits in different regions have been performed, assuming the usual exponential decay distribution for the signal. In these fits, background events are treated like the signal: only one fit parameter, which represents the mean lifetime of the decay, is assumed in the likelihood function. The fit range is limited to the region where trigger and selection efficiencies are large: 0.9 – 8.5 ps. Since the efficiency is not constant in this range, its variation is included in the fitting model, by weighting each event by the reciprocal of its detached vertex selection efficiency. The results of the fits are summarized in Table III.

For detached candidates in the J/ψ mass range ($[3.0, 3.2]$ GeV/c^2 in the muon channel and $[2.9, 3.2]$ GeV/c^2 in the electron channel), the mean lifetime is 1.61 ± 0.27 ps and 1.21 ± 0.18 ps for dimuons and dielectrons, respectively, in agreement with the value obtained from generated and reconstructed MC b decays: 1.56 ± 0.01 ps. Background regions in data (side bands in the invariant mass spectrum and upstream events) usually have lower mean lifetime values and larger uncertainties due to the poorer statistics.

For reference we also measure the mean lifetime of the main background channels described by MC. As expected, the open $c\bar{c}$ events generally have a lower lifetime, while the semileptonic $b\bar{b}$ events behave differently depending on the invariant mass range of the dilepton. The higher mass range is dominated by combinations of leptons from two different b decay branches, while, in the low mass range, dileptons from the decay chain of a single b quark dominate. The mean lifetime measured in the latter sample is clearly close to that of the b .

To improve the statistical accuracy of the lifetime measurement, a joint unbinned likelihood fit is performed on the muon and electron candidates (104 events in total). This sample is highly enriched in b content,

Sample	Mass Range (GeV/c ²)	$\tau_{\mu\mu}$ (ps)	τ_{ee} (ps)
data downstream	J/ψ region	1.61 ± 0.27	1.21 ± 0.18
$b \rightarrow J/\psi$ MC	J/ψ region	1.55 ± 0.01	1.57 ± 0.01
data downstream	2.0–2.5	1.30 ± 0.16	0.86 ± 0.09
data downstream	3.6–12.0	0.55 ± 0.13	0.54 ± 0.21
data upstream	2.0–12.0	1.08 ± 0.21	1.16 ± 0.19
$b\bar{b}$ semileptonic MC	2.0–2.5	1.47 ± 0.12	1.45 ± 0.04
$b\bar{b}$ semileptonic MC	3.6–12.0	0.71 ± 0.09	0.67 ± 0.03
$c\bar{c}$ double semileptonic MC	2.0–12.0	0.47 ± 0.06	0.30 ± 0.02

TABLE III: Results of the unbinned maximum likelihood fits on the detached $\mu^+\mu^-$ and e^+e^- candidates in real data and on various MC samples. The J/ψ mass range is defined as for Fig. 6.

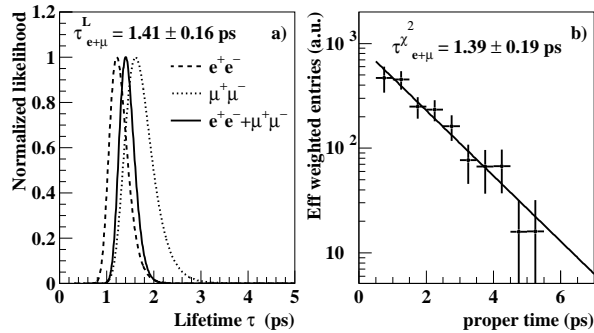


FIG. 7: a) Likelihoods for the $\mu^+\mu^-$ and e^+e^- detached candidate fits and joint likelihood as a function of the mean lifetime; b) distribution of proper times for the detached J/ψ events corrected for selection efficiency.

having about 80 $b \rightarrow J/\psi$ candidates plus about 10 events coming from semileptonic b decays. A value of $\tau_{e^+\mu}^L = 1.41 \pm 0.16$ ps is obtained (see Fig. 7a). Since the total number of candidates is sufficiently large, a standard χ^2 fit is also performed on the efficiency-corrected distribution of proper times for the same events (see Fig. 7b). In this case, the minimum χ^2 ($\chi^2/\text{ndf} = 5.1/8$) is obtained for $\tau_{e^+\mu}^{\chi^2} = 1.39 \pm 0.19$ ps. Both results are in good agreement with the expected value for b hadrons.

B. $J/\psi + h^\pm$ analysis

As described in Sect. VI, rather strong (and therefore relatively inefficient) detachment cuts are necessary to do an inclusive selection of $b \rightarrow J/\psi$ decays. A partially different sample of b events can be obtained by relaxing the detachment cuts and imposing additional requirements on other quantities which characterize b hadron decays, for example requiring the presence of a third track h^\pm forming a good vertex with the J/ψ candidate. Since the J/ψ carries most of the b hadron momentum, the additional track usually has low momentum and points far away from the primary interaction. This selection gives access to b events with smaller detachment from the target wire, but nevertheless provides high purity because of the stringent requirements on the three-prong decay vertex (which has an intrinsically lower background).

For events with dimuon candidates selected as described in Sect. V, a search is made for additional decay products among good quality tracks nearby the J/ψ vertex. The presence of a third track, whose closest distance of approach to the primary vertex is larger than 300 μm is required. Detachment cuts are then applied, and the requirements summarized in Table I are relaxed. In particular the minimum Δz significance is reduced to 5σ , and the minimum lepton impact parameter to the target wire is lowered to 2σ .

The dilepton invariant mass and mass vs proper time distribution of events selected in the muon sample are shown in Fig. 8. A J/ψ peak is clearly visible, with an improved signal-to-background ratio with respect to the detached J/ψ analysis of Sect. VI, Fig. 4. From the unbinned maximum likelihood fit, the number of

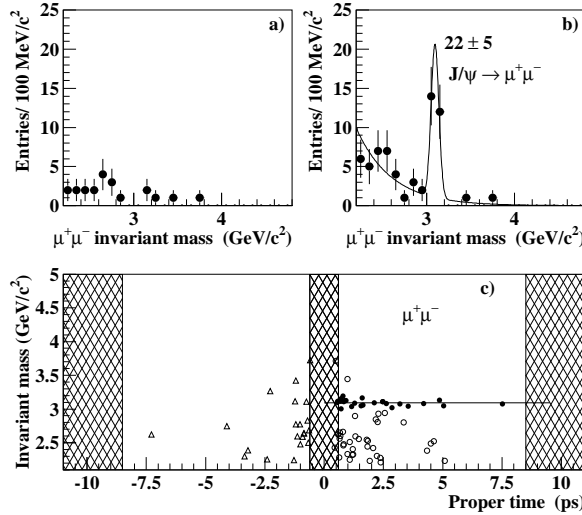


FIG. 8: $\mu^+\mu^-$ invariant mass for the $J/\psi + h^\pm$ analysis for upstream (a) and downstream (b) events. The line in (b) shows the result of the unbinned max likelihood fit. c) $\mu^+\mu^-$ invariant mass as a function of the proper time for the detached candidates.

detached J/ψ events is $n_{b\bar{b}} = 22 \pm 5$. Only 50% of these events are in common with the previous detached vertex analysis.

Using these selected events, another value of the cross section ratio in our acceptance, $R_{\Delta\sigma} = \Delta\sigma(b\bar{b})/\Delta\sigma_{J/\psi} = 0.043 \pm 0.010$, was obtained. The measurement is compatible with both the muon and the electron results presented in Sect. VI (within 0.6σ from the electron value, obtained with a statistically independent sample). Since it is partly correlated with the muon result of Sect. VI B, it is not combined into the final cross section results presented in Sect. VIII.

C. Other Studies

Further confirmation of the b flavor content of the detached J/ψ sample has been obtained from other analyses. We studied the kaon population and the distribution of high p_T tracks. For muon events and for two-BR tag electron events falling in an invariant mass window around the J/ψ , we observed that the real data after prompt selection behave as the prompt J/ψ MC candidates, while after the detachment selection larger values of both, the p_T distribution and the kaon population, are found, compatible with the $b \rightarrow J/\psi$ MC sample.

A search for the exclusive decays $B^+ \rightarrow J/\psi K^+$ and $B^0 \rightarrow J/\psi K^+ \pi^-$ has been made. A few fully reconstructed B meson candidates are found, both for the muon and the electron channels, but not sufficient for a full exclusive analysis.

The kinematic characteristics of the detached J/ψ candidates have been checked against the production model employed to evaluate the efficiencies and were found to be compatible in our x_F and p_T acceptance.

VIII. COMBINED CROSS SECTION MEASUREMENT

The two measurements of $\Delta\sigma(b\bar{b})/\Delta\sigma_{J/\psi}$, presented in Eqs. (3) and (4), are statistically independent and compatible. To have a more precise measurement of $R_{\Delta\sigma}$, a joint unbinned maximum likelihood fit is performed on the detached $\mu^+\mu^-$ and e^+e^- candidates, using $R_{\Delta\sigma}$ and all background terms (n_{bkg} and λ for the two channels) as free parameters. In Fig. 9, the likelihoods of the invariant mass fits are shown for $\mu^+\mu^-$ and e^+e^- separately and for the combined fit. The fit provides the final value

$$R_{\Delta\sigma} = \frac{\Delta\sigma(b\bar{b})}{\Delta\sigma_{J/\psi}} = 0.0314 \pm 0.0049_{\text{stat}}$$

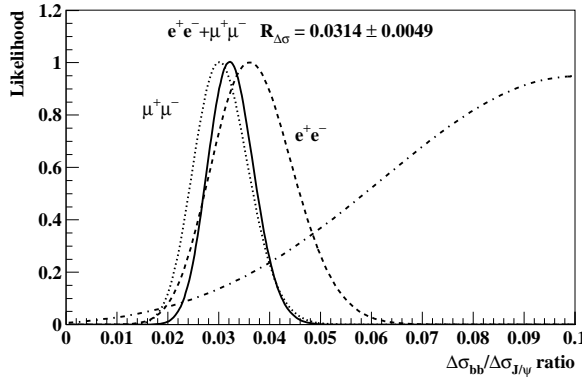


FIG. 9: Likelihoods of the invariant mass fits as a function of $R_{\Delta\sigma}$, shown separately for $\mu^+\mu^-$ data (dotted line), e^+e^- data (dashed line) and for the combination of the two (continuous line). The dot-dashed line shows the likelihood function corresponding to the 2000 data analysis [10] which is used in the final average.

where the quoted uncertainty (15%) is dominated by the statistical fluctuations on the detached J/ψ counting and contains the statistical contributions from the prompt J/ψ counting ($\approx 1\%$), the efficiencies ($\approx 5\%$) and the α exponent ($\approx 1\%$).

The main sources of systematic uncertainties³, which are not related to the $b\bar{b}$ statistics, are due to the $\text{Br}(b\bar{b} \rightarrow J/\psi X)$ (8.6%), to the trigger and reconstruction efficiency ratio ε_R (5%), to the b production and decay model (5%), to the prompt J/ψ production model (3.1%) and to the prompt J/ψ counting (1.5%). Other contributions are below the 1% level. To determine the sensitivity of the results to the cut values, we vary them within reasonable ranges, always requiring a negligible prompt J/ψ background. A conservative estimate of 5% systematic uncertainty has been obtained. The uncertainties in the background shape and yield give a negligible contribution to the systematic uncertainty (below 1%) in the muon channel but a sizeable contribution in the electron channel (7%). The overall systematic uncertainty for the two channel average measurement is 14%.

The weighted averages of the muon and electron results for the different target materials and for the total are presented in Table IV. As can be seen from the χ^2 probability, the two channels are always compatible. The three $\frac{\Delta\sigma_{bb}^A}{\Delta\sigma_P^A}$ measurements are also compatible with the assumed linear A dependence of the $b\bar{b}$ cross section.

The present result is $1.7\sigma_{\text{stat}}$ below the previous HERA-B measurement [10] ($R_{\Delta\sigma} = 0.107 \pm 0.047_{\text{stat}} \pm 0.022_{\text{sys}}$) which was obtained with a similar technique but with a much smaller data sample (dot-dashed line in Fig. 9). Since the two data samples are independent, we combine the two measurements assuming that the systematic errors are uncorrelated. We obtain:

$$R_{\Delta\sigma} = \frac{\Delta\sigma(b\bar{b})}{\Delta\sigma_{J/\psi}} = 0.032 \pm 0.005_{\text{stat}} \pm 0.004_{\text{sys}}. \quad (5)$$

Material (A)	$N_{J/\psi}$	$n_{b\bar{b}}$	σ ratio	value	$\text{Prob}(\chi^2)$
Carbon (12)	161 k	45.6 ± 8.4		0.0324 ± 0.0059	94%
Titanium (48)	13 k	3.9 ± 2.3	$\Delta\sigma_{bb}^A/\Delta\sigma_P^A$	0.027 ± 0.018	54%
Tungsten (184)	78 k	33.9 ± 7.6		0.044 ± 0.010	29%
Total	251k	83 ± 12	$\Delta\sigma(b\bar{b})/\Delta\sigma_{J/\psi}$	0.0314 ± 0.0049	54%

³ The quoted systematic uncertainties correspond to a 1σ interval and are usually evaluated as the maximal interval width of the cross section variation divided by $\sqrt{12}$.

TABLE IV: Combined $\mu^+\mu^-$ and e^+e^- results: sum of the number of prompt ($N_{J/\psi}$) and detached J/ψ ($n_{b\bar{b}}$) found for the two channels together, $\Delta\sigma_{b\bar{b}}^A/\Delta\sigma_P^A$ (rows 1–3), $\Delta\sigma(b\bar{b})/\Delta\sigma_{J/\psi}$ (row 4), and χ^2 probability of the average value.

To compare our result with other measurements and theoretical predictions, we extrapolate the $R_{\Delta\sigma}$ ratio to the full kinematic range and then make use of the value of $\sigma_{J/\psi}$ presented in Sect. II, obtaining the $\sigma(b\bar{b})$ value:

$$\sigma(b\bar{b}) = 14.9 \pm 2.2_{\text{stat}} \pm 2.4_{\text{sys}} \text{ nb/nucleon.} \quad (6)$$

This result can be compared with the available measurements, which were obtained in $p\text{Au}$ [8] and $p\text{Si}$ [9] collisions at 800 GeV/c proton momentum. Due to the near-threshold conditions in which all experiments (including HERA-B) operated, it is necessary to rescale the Fermilab results for the different \sqrt{s} value of the collision. The latest QCD calculations predict an increase of the $b\bar{b}$ cross section between 800 (Fermilab) and 920 GeV/c (HERA-B) by $(42 \pm 9)\%$ [6, 7]. All the available measurements are presented in Table V, where a scaling of the Fermilab measurements to HERA-B energies is performed. As can be seen, the present result (Eq. 6) is consistent with both the E789 value (within 1.6σ) and with the E771 value (within 1.8σ).

Experiment	Year	Target	p (GeV/c)	Events	$\sigma(b\bar{b})$ (nb/nucleon)	$\sigma(b\bar{b})$ at 920 GeV/c	Ref.
E789	1995	Au	800	19	$5.7 \pm 1.5 \pm 1.3$	$8.1 \pm 2.2 \pm 1.9$	[8]
E771	1999	Si	800	15	$43_{-17}^{+27} \pm 7$	$61_{-24}^{+38} \pm 11$	[9]
HERA-B	2002	C/Ti	920	10	$32_{-12}^{+14} \pm 6$ (*)	$32_{-12}^{+14} \pm 6$ (*)	[10]
HERA-B	2005	C/Ti/W	920	83	$14.4 \pm 2.2 \pm 2.3$	$14.4 \pm 2.2 \pm 2.3$	t.w.
HERA-B	2002/5	C/Ti/W	920	93	$14.9 \pm 2.2 \pm 2.4$	$14.9 \pm 2.2 \pm 2.4$	t.w.

TABLE V: Present experimental situation on the $b\bar{b}$ cross section in pN interactions with the comparison of all the measurements rescaled at 920 GeV/c proton momentum.

(*) Value as quoted in the paper, which was obtained using a $\sigma_{J/\psi}$ value different from the current paper.

The measurements presented in Table V can also be compared to the latest QCD predictions [6, 7], which have been performed by two theory groups. They both employ Next-to-Leading-Order (NLO) calculations with resummation techniques to take into account the large corrections due to emission of soft gluons. The calculations give $\sigma(b\bar{b}) = 28 \pm 15$ nb/nucleon [7] and $\sigma(b\bar{b}) = 25_{-13}^{+20}$ nb/nucleon [47]: the results are shown in Fig. 10 as a function of \sqrt{s} . As can be seen, the present measurement is compatible with the theoretical calculations.

IX. CONCLUSIONS

A search for $b \rightarrow J/\psi X \rightarrow l^+l^-X$ decays has been performed on a sample of 164 million dilepton trigger events, acquired during the HERA-B 2002–2003 physics run. The data analysis, based on identification of detached vertices, resulted in 46.2 ± 8.2 $b \rightarrow J/\psi X \rightarrow \mu^+\mu^-X$ candidates and 36.9 ± 8.1 $b \rightarrow J/\psi X \rightarrow e^+e^-X$ candidates.

From these events, we measure the ratio $\Delta\sigma(b\bar{b})/\Delta\sigma_{J/\psi}$ of the $b\bar{b}$ production cross section to the prompt J/ψ cross section in the HERA-B acceptance range ($-0.35 < x_F < 0.15$). Within statistical uncertainties, the results for the muon and for the electron channel are compatible and yield a combined value of $\Delta\sigma(b\bar{b})/\Delta\sigma_{J/\psi} = 0.0314 \pm 0.0049_{\text{stat}} \pm 0.0044_{\text{sys}}$, where the systematic uncertainty (14%) is dominated by the 8.6% contribution due to the branching fraction $\text{Br}(b\bar{b} \rightarrow J/\psi X)$. The present measurement is then combined with the HERA-B 2000 measurement [10], for a final result of:

$$R_{\Delta\sigma} = \frac{\Delta\sigma(b\bar{b})}{\Delta\sigma_{J/\psi}} = 0.032 \pm 0.005_{\text{stat}} \pm 0.004_{\text{sys}}. \quad (7)$$

Further investigations of the detached vertex sample confirm the b nature of the candidates. The measured mean lifetime $\tau = 1.41 \pm 0.16$ ps agrees well with previous measurements of the average b lifetime [11]. A

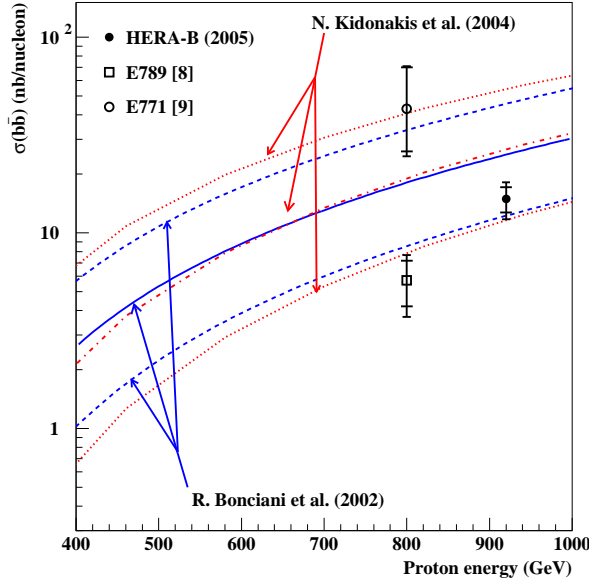


FIG. 10: Comparison of the available $\sigma(b\bar{b})$ measurements with the theoretical predictions of R. Bonciani *et al.* [6] updated with the NNLO parton distribution function in [39] (solid line: central value, dashed lines: upper and lower bounds) and N. Kidonakis *et al.* [7] (dot-dashed line: central value, dotted lines: upper and lower bounds). The upper and lower bounds have been defined by changing the renormalization and factorization scales (by a factor 0.5 and 2.0) and the b quark mass ($4.5 - 5.0$ GeV/ c^2).

search for extra tracks coming from the detached J/ψ vertex in the muon channel yields 22 ± 5 partially reconstructed $b \rightarrow J/\psi + h^\pm + X$ events. From this latter sample, 50% of which consists of detached J/ψ mesons not found in the inclusive analysis, a $R_{\Delta\sigma}$ cross section ratio in good agreement with the main measurement is obtained. In addition to these checks, we have verified that the detached candidate events have a kaon and p_T distribution that is in good agreement with that expected for b events.

To compare our result to previous measurements and to theoretical calculations, we compute the $\sigma(b\bar{b})$ cross section by extrapolating the ratio $R_{\Delta\sigma}$ to the full phase space and using the value of $\sigma_{J/\psi} = (502 \pm 44)$ nb/nucleon [13]. The resulting $\sigma(b\bar{b})$ cross section is $14.9 \pm 2.2_{\text{stat}} \pm 2.4_{\text{sys}}$ nb/nucleon. Comparing to the other available experimental results, the present value is within 1.6σ of the E789 value [8] (after rescaling to the same \sqrt{s}) and 1.8σ below the rescaled E771 measurement [9].

The HERA-B value can be compared with the latest QCD predictions, calculated beyond the NLO order and considering the effects of soft-gluon re-summation, performed at 920 GeV/ c proton momentum. Our result is within 1σ of the current calculations [7, 47].

Acknowledgments

We express our gratitude to the DESY laboratory for the strong support in setting up and running the HERA-B experiment. We are also indebted to the DESY accelerator group for the continuous efforts to provide good and stable beam conditions. The HERA-B experiment would not have been possible without the enormous effort and commitment of our technical and administrative staff. It is a pleasure to thank all of them.

In the preparation of this paper we have benefitted from many useful discussions with M. Mangano, N. Kidonakis, P. Nason and R. Vogt on the theory of $b\bar{b}$ production, and with F. Maltoni on the J/ψ

hadroproduction models.

[1] M. Cacciari, Nucl. Phys. **B** **135** (Proc. Suppl.) (2004) 61;
 M. Cacciari, hep-ph/0407187.

[2] S. Frixione, Proceeding of the DIS 04 conference, hep-ph/0408317.

[3] S. Frixione *et al.*, Adv. Ser. Direct. High Energy Phys. **15** (1998), 609.

[4] G. P. Salam, Acta Phys. Polon. **B33** (2002) 2791, hep-ph/0207147.

[5] H. Wohri and C. Lourenco, J. Phys. **G30** (2004) S315-S324.

[6] R. Bonciani *et al.*, Nucl. Phys. **B529** (1998) 424.

[7] N. Kidonakis and R. Vogt, Eur. Phys. J. **C36** (2004) 201;
 N. Kidonakis *et al.*, Phys. Rev. **D64** (2001) 114001.

[8] D. M. Jansen *et al.*, Phys. Rev. Lett. **74** (1995) 3118.

[9] T. Alexopoulos *et al.*, Phys. Rev. Lett. **82** (1999) 41.

[10] I. Abt *et al.*, Eur. Phys. J. **C26** (2003) 345.

[11] S. Eidelman *et al.*, Phys. Lett. **B592** (2004) 1.

[12] M. J. Leitch *et al.*, Phys. Rev. Lett. **84** (2000) 3256.

[13] M. Bargiotti *et al.*, "Analysis of charmonium production at fixed-target experiments in the NRQCD approach", in preparation; Hera-B internal note 05-015.

[14] I. Abt *et al.*, "Measurement of the J/ψ Production Cross Section in 920 GeV/c Fixed-Target Proton-Nucleus Interactions", Preprint DESY 05-232, hep-ex/0512029, submitted to Phys. Lett. B.

[15] R. Vogt, Int. J. Mod. Phys. **E12** (2003) 211.

[16] M. J. Leitch *et al.*, Phys. Rev. Lett. **72** (1994) 2542.

[17] E. Hartouni *et al.*, HERA-B Design Report, DESY-PRC-95-01 (1995).

[18] The HERA-B Collaboration, HERA-B Status Report, DESY-PRC-00-04 (2000).

[19] K. Ehret, Nucl. Instr. Methods **A446** (2000) 190.

[20] C. Bauer *et al.*, Nucl. Instr. Methods **A501** (2003) 39.

[21] T. Zeuner, Nucl. Instr. Methods **A446** (2000) 324;
 Y. Bagaturia *et al.*, Nucl. Instr. Methods **A490** (2002) 223.

[22] H Albrecht *et al.*, Nucl. Instr. Methods **A541** (2005) 610;
 H Albrecht *et al.*, arXiv/physics/0507048, DESY 05-99, submitted to Nucl. Instr. Meth. A.

[23] J. Pyrlik, Nucl. Instr. Methods **A446** (2000) 299;
 I. Ariño *et al.*, Nucl. Instr. Methods **A453** (2000) 289.

[24] G. Avoni *et al.*, Proc. of the IX Conference on Calorimetry in Particle Physics, Annecy, France, October 9–14, 2000, Calorimetry in High energy physics, (2001) 777;
 A. Zoccoli, Nucl. Instr. Methods **A446** (2000) 246.

[25] B. Giacobbe, Nucl. Phys. **B** **150** (Proc. Suppl.) (2006) 257.

[26] M. Buchler *et al.*, IEEE Trans. on Nucl. Sci. **46** (1999) 126;
 A. Arefiev *et al.*, IEEE Trans. on Nucl. Sci. **48** (2001) 1059.

[27] M. Böcker *et al.*, IEEE Trans. Nucl. Sci. **48** (2001) 1270;
 Yu. Gilitsky *et al.*, Nucl. Instr. Methods **A461** (2001) 104.

[28] V. Alberico *et al.*, Il Nuovo Cimento, **110 A** (1997) 1453;
 G. Avoni *et al.*, Nucl. Instr. Methods **A461** (2001) 332.

[29] V. Balagura *et al.*, Nucl. Instr. Methods **A494** (2002) 526.

[30] T. Núñez *et al.*, Nucl. Phys. **B120** (proc. suppl.) (2003) 166;
 P. Kreuzer, Nucl. Instr. Methods **A462** (2001) 212.

[31] M. Dam *et al.*, Nucl. Instr. Methods **A525** (2004) 566.

[32] T. Sjöstrand, Comp. Phys. Comm. **82** (1994) 74.

[33] H. Pi, Comp. Phys. Comm. **71** (1992) 173.

[34] R. Brun *et al.*, GEANT3, Internal Report CERN DD/EE/84-1, CERN, 1987.

[35] T. Alexopoulos *et al.*, Phys. Rev. **D55** (1997) 3927.

[36] J. Spengler, J. Phys. **G30** (2004) S871.

[37] E. J. Siskind *et al.*, Phys. Rev. **D21** (1980) 628; A. Gribushin *et al.*, Phys. Rev. **D62** (2001) 012001; T. H. Chang *et al.*, Phys. Rev. Lett. **91** (2003) 211801.

[38] M. Mangano, P. Nason and G. Ridolfi, Nucl. Phys. **B373** (1992) 295;
 P. Nason, S. Dawson and R. K. Ellis, Nucl. Phys. **B327** (1988) 49.

[39] A. D. Martin *et al.*, Phys. Lett. **B531** (2002) 216.

[40] J. Chay, S. D. Ellis and W. J. Stirling, Phys. Rev. **D45** (1992) 46.

[41] C. Peterson *et al.*, Phys. Rev. **D27** (1983) 105.

[42] J. Chrin, Z. Phys. **C36** (1987) 163;
 D. Decamp *et al.*, Phys. Lett. **B244** (1990) 551;

P. Nason and C. Oleari, Nucl. Phys. **B565** (2000) 245.

[43] H. L. Lai *et al.*, Eur. Phys. J. **C12** (2000) 375.

[44] A. Heister *et al.*, Phys. Lett. **B512** (2001) 30.

[45] V. G. Kartvelishvili, A. K. Likhoded and V. A. Petrov, Phys. Lett. **B78** (1978) 615.

[46] A. Spiridonov, hep-ex/0510076, DESY-04-105.

[47] P. Nason, Private communication.